Beyond-mean-field calculations of collectivities of neutron-rich Fe and Cr isotopes

C. F. Jiao (焦长峰),[1] J. C. Pei (裴俊琛),[1,2] and F. R. Xu (许甫荣)[1,2,*]

[1]*State Key Laboratory of Nuclear Physics and Technology, School of Physics, Peking University, Beijing 100871, China*

[2]*State Key Laboratory of Theoretical Physics, Institute of Theoretical Physics, Chinese Academy of Sciences, Beijing 100190, China*

(Received 28 July 2014; revised manuscript received 2 October 2014; published 12 November 2014)

The rotational symmetry is broken in mean-field models. The symmetry breaking may lead to significant effects even on the ground states of nuclei. The recent observations of enhanced collectivities in neutron-rich Fe and Cr isotopes are challenging the current calculations of mean-field models. By performing angular-momentum projection on mean-field potential energy surface (PES), we can obtain an angular-momentum-conserved PES at each given spin. With the projected PES, we have investigated the collectivity of neutron-rich Fe and Cr isotopes. The calculations reproduce well the excitation energies and electric quadrupole transitions of the collective excited states of the isotopes, indicating the importance of the restoration of the rotational symmetry.

DOI: 10.1103/PhysRevC.90.054314 PACS number(s): 21.10.−k, 21.60.−n, 27.40.+z, 27.50.+e

I. INTRODUCTION

Mean-field approaches have achieved remarkable success in understanding nuclear properties, especially for the collectivities of deformed nuclei [1]. However, the deformed mean-field wave function breaks necessarily the rotational symmetry. It results in spurious overlaps between the ground state and excited configurations. For example, the zero-point energy correction associated with the recovery of the rotational symmetry is somehow proportional to deformation, ranging from a few keV for nearly spherical configurations to several MeV for well-deformed states [2,3]. For a shape-soft nucleus, i.e., with a flat potential-energy surface (PES) with respect to deformation, the energy correction could be quantitatively comparable to the energy differences between different shapes and thus it topologically alters the PES [3,4]. Therefore, one may expect that the beyond-mean-field effect stemming from the restoration of the rotational symmetry is of significant importance in describing the collectivities of soft nuclei [5].

Recently, experiments observed low-lying 2_1^+ states [6–8] with increased deformation lengths δ [9] and large $E2$ transition probabilities $B(E2;0_1^+ \rightarrow 2_1^+)$ [10–13] in neutron-rich Fe and Cr isotopes, indicating enhanced collectivities. However, mean-field calculations showed that quadrupole deformations decrease rapidly when the neutron number approaches $N = 40$ in Fe and Cr isotopes [14–16], implying fewer collectivities. In these mean-field calculations, flat PES's with shallow minima were obtained, see, e.g., Ref. [17]. As noted, the influence from symmetry breaking would be significant for soft nuclei.

In the present work, we want to see what effects may be brought by the recovery of the rotational symmetry. Starting from a simple mean-field model, we employ the angular-momentum projection technique to restore the rotational symmetry. Though the sophisticated calculations of the angular-momentum projection based on the Skyrme- [4] or Gogny-type mean field [18,19] have been performed, these calculations have not included multiquasiparticle (multi-qp) components in the wave functions. The multi-qp configurations break the time-reversal symmetry, raising a time-odd term in mean-field models, which increases the difficulty for the projection calculation. However, multi-qp configurations are important for the descriptions of excited states [20]. It was noted that the overestimated energies of low-lying states calculated in Refs. [5,19] would be due to the absence of the components with the time-reversal symmetry breaking [19].

To include the multi-qp configurations, the angular-momentum projection performed within the Nilsson model has a significant advantage for simplicity, which is called the projected shell model (PSM) [21–25]. However, the existing PSM applies to deformation-fixed calculations, i.e., assuming a fixed deformation in calculations. In principle, the deformation-variation effect can be well included in the PSM by configuration mixing if the model space taken is large enough. In order to include effects from both shape variation and multi-qp components, we have explored the angular-momentum projection calculation within the framework of the simple macroscopic-microscopic (MM) model. It has been well known that the PES calculated by the MM model is one of the most powerful tools to predict nuclear shapes. By performing the angular-momentum projection, we can obtain an angular-momentum-conserved PES. Such a projected energy surface method has been suggested also by Tu and her coauthors, investigating a well-deformed nucleus, ^{172}W [26].

II. THE MODEL

The details of the PSM can be found in Refs. [21,27]. To avoid the spurious pairing collapse encountered in the Bardeen-Cooper-Schrieffer (BCS) method which is used in the existing PSM, we have improved the pairing treatment by using the Lipkin-Nogami approach. As commented, the inclusion of excited qp configurations is important. In the present calculation of even-even nuclei, the configurations considered include zero-qp, two-quasineutron, two-quasiproton, and four-qp (two quasineutrons plus two quasiprotons) components, i.e., $\{|\Phi_\xi\rangle\} = \{|0\rangle, a^\dagger_{\nu_i} a^\dagger_{\nu_j}|0\rangle, a^\dagger_{\pi_i} a^\dagger_{\pi_j}|0\rangle, a^\dagger_{\nu_i} a^\dagger_{\nu_j} a^\dagger_{\pi_k} a^\dagger_{\pi_l}|0\rangle\}$, where $|0\rangle$ is the qp vacuum. The PSM many-body wave function can

*frxu@pku.edu.cn

be expressed in terms of various projected configurations [21],

$$|\Psi^I\rangle = \sum_\xi f_\xi^I \hat{P}_{MK}^I |\Phi_\xi\rangle, \quad (1)$$

where $\hat{P}_{MK}^I$ is the angular-momentum projection operator. $|\Phi_\xi\rangle$ denotes a mean-field configuration (before projection), and the coefficient f_ξ^I is the corresponding weight factor which is obtained by diagonalizing the eigenvalue equation,

$$\sum_{\xi'} \left(H_{\xi\xi'}^I - E^I N_{\xi\xi'}^I\right) f_{\xi'}^I = 0, \quad (2)$$

where $H_{\xi\xi'}^I$ and $N_{\xi\xi'}^I$ are the matrix elements of the Hamiltonian and the norm, respectively, defined by

$$H_{\xi\xi'}^I = \langle\Phi_\xi|\hat{H}\hat{P}_{K_\xi K_{\xi'}}^I|\Phi_{\xi'}\rangle, \quad N_{\xi\xi'}^I = \langle\Phi_\xi|\hat{P}_{K_\xi K_{\xi'}}^I|\Phi_{\xi'}\rangle. \quad (3)$$

The weight factor f_ξ^I reflects the mixing amplitudes of different qp configurations. An axially symmetric shape is assumed, and thus each basis state can be labeled by the good quantum number of the spin projection K onto the symmetry axis. The state $|\Psi^I\rangle$ is a linear superposition of various K states, i.e., K mixing.

The Hamiltonian takes the following form, which includes the quadrupole-quadrupole (QQ) interaction and the monopole plus quadrupole pairings [21],

$$\hat{H} = \hat{H}_0 - \frac{\chi}{2}\sum_\mu \hat{Q}_{2\mu}^\dagger \hat{Q}_{2\mu} - G_M \hat{P}^\dagger \hat{P} - G_Q \sum_\mu \hat{P}_{2\mu}^\dagger \hat{P}_{2\mu}, \quad (4)$$

where $\hat{H}_0 = \sum_\alpha e_\alpha c_\alpha^\dagger c_\alpha$ with e_α for spherical Nilsson single-particle energies [21]. The monopole-pairing strength G_M is determined by the average gap method [28]. The quadrupole-pairing strength G_Q is taken to be proportional to G_M, with a constant factor of 0.24, i.e., $G_Q = 0.24 G_M$. We will discuss the strength χ of the QQ interaction in more detail later.

In the PSM calculations, one usually needs a cutoff of the model space to reduce the computational task. The existing PSM considers three major Nilsson shells in calculations [21]. This means that the energy $\langle\Psi^I|\hat{H}|\Psi^I\rangle$ given by the PSM wave function $|\Psi^I\rangle$ in Eq. (1) is not the total energy of the nucleus but the energy of the valence particles. We can well assume that the angular momentum of an excited state is generated by the valence particles, but the total energy (not only the energy of valence particles) should be used in the determination of nuclear shape by minimizing the energy against deformations. In the MM model, nuclear shape can be obtained by plotting the total energy surface. This similar method has also been adopted in the cranking shell model in which the total energy (in the body-fixed frame) of a rotational state is written as the total energy of the nucleus at rest and the energy change due to rotation [29,30]. Similarly, only the valence particles are taken into account in cranking calculations. With comparisons above, we can write the projected total energy for an excited state at spin I as

$$E^I(N,Z,\hat{\beta}) = E_{\rm MM}(N,Z,\hat{\beta}) + E_{\rm rot}^I(N,Z,\hat{\beta}), \quad (5)$$

where $\hat{\beta}$ represents a set of deformation parameters. $E_{\rm MM}(N,Z,\hat{\beta})$ is the total energy of the nucleus at rest, which can be calculated by the MM model, including the macroscopic energy, the microscopic shell correction, and the pairing energy in the standard Strutinsky method. $E_{\rm rot}^I(N,Z,\hat{\beta})$ gives the energy gain due to rotation (including possible intrinsic excitation energy if the rotational state has, e.g., a broken-pair intrinsic structure), defined by

$$E_{\rm rot}^I = \frac{\langle\Psi^I|\hat{H}|\Psi^I\rangle}{\langle\Psi^I|\Psi^I\rangle} - \frac{\langle 0|\hat{H}|0\rangle}{\langle 0|0\rangle}. \quad (6)$$

The first term is the energy of the valence-particle system at spin I (with a given intrinsic structure), which is calculated by the projected wave function $|\Psi^I\rangle$. The second term is the energy of the valence-particle system before angular-momentum projection, which is calculated by the unprojected qp vacuum $|0\rangle$. Note that the energy $E_{\rm rot}^I$ is not equal to zero even for the $I = 0$ ground state of an even-even nucleus. For the ground-state case, it is in fact an energy correction due to the restoration of the rotational symmetry. This energy correction can be sensitive to deformation and therefore would play a significant role in the determinations of nuclear shapes, even for the ground state. In the present calculations, the macroscopic energy is calculated by the new version of the liquid-drop model (called new liquid drop (NLD) in Ref. [31]) with the inclusion of a Gauss-curvature term, which takes the following form [31]:

$$\begin{aligned} &E_{\rm mac}(N,Z,\hat{\beta}) \\ &= b_{\rm vol}(1-\kappa_{\rm vol}I^2)A + b_{\rm surf}(1-\kappa_{\rm surf}I^2)A^{2/3}B_{\rm surf}(\hat{\beta}) \\ &\quad + b_{\rm curG}(1-\kappa_{\rm curG}I^2)A^0 + \frac{3}{5}e^2\frac{Z^2}{r_0^{ch}A^{1/3}}B_{\rm Coul}(\hat{\beta}) \\ &\quad - C_4\frac{Z^2}{A} + E_{\rm W}, \end{aligned} \quad (7)$$

where $I = (N-Z)/A$. $b_{\rm vol}$, $\kappa_{\rm vol}$, $b_{\rm surf}$, $\kappa_{\rm surf}$ $b_{\rm curG}$, $\kappa_{\rm curG}$, $r_0^{\rm ch}$, and C_4 are the liquid-drop model parameters. The Wigner term $E_{\rm W}$ is given as $E_{\rm W} = -10\exp(-42|I|/10)$ according to Refs. [31,32].

The PES is calculated in the (β_2,β_4) deformation space. In the deformation-fixed PSM calculations, the QQ interaction strength χ is determined by the assumption that the PSM Hamiltonian gives the same QQ interaction as that derived from the Nilsson model [21]. In the present calculations, we obtain a χ value at each deformation point of the (β_2, β_4) lattice using the method above. At the same time we can obtain the PES of the ground state which is analyzed for the determination of the χ parameter. Note that the χ value obtained thus can change slightly with changing deformation in the PES lattice. We assume that the χ value obtained at the PES minimum (i.e., at the deformation of the ground state) should be the most reasonable value. With such a χ value, we perform the deformation-variable PSM calculations, obtaining the projected PES for each given angular momentum. The excitation energy and deformation at a given spin are obtained by minimizing the corresponding projected PES. Several different PES's at the same spin I may be obtained, corresponding to different intrinsic configurations.

Before practical calculations, we thought that the liquid-drop model parameters were determined by fitting data without

TABLE I. The parameter readjustments of the new version of liquid-drop model [31]. The NLD parameters are the original values of the parameters given in Ref. [31].

Parameters	Present work	NLD
$b_{\rm vol}$ (MeV)	−15.4920	−15.4721
$\kappa_{\rm vol}$	1.6410	1.6411
$b_{\rm surf}$ (MeV)	16.3879	17.0603
$\kappa_{\rm surf}$	0.4545	0.7546
$b_{\rm curG}$ (MeV)	26.0575	10.3574
$\kappa_{\rm curG}$	8.0876	13.4235
$r_0^{\rm ch}$ (fm)	1.19599	1.21610
C_4 (MeV)	0.9124	0.7952

the restoration of the rotational symmetry [31]. In the present work, we readjust the liquid-drop model parameters in order to include possible effects from the restoration of the rotational symmetry. At each readjustment of the parameters, we perform a projected PES calculation for the ground state, which gives both the χ determination and binding energy (at the readjusted parameters). Then the final values of optimized parameters are determined by fitting experimental binding energies. The projected PES calculations are computationally time-consuming. We selected about 150 nuclei which cover the Cr and Fe mass region, mass ∼180, and actinide regions for the parameter readjustments. The refitting result gives a root-mean-square deviation of 0.725 MeV for the ground-state binding energies between the calculations and data (taken from Ref. [33]). The readjusted parameters are listed in Table I, compared with the NLD parameters of Ref. [31]. As a further test of the readjusted parameters and projected PES's, we

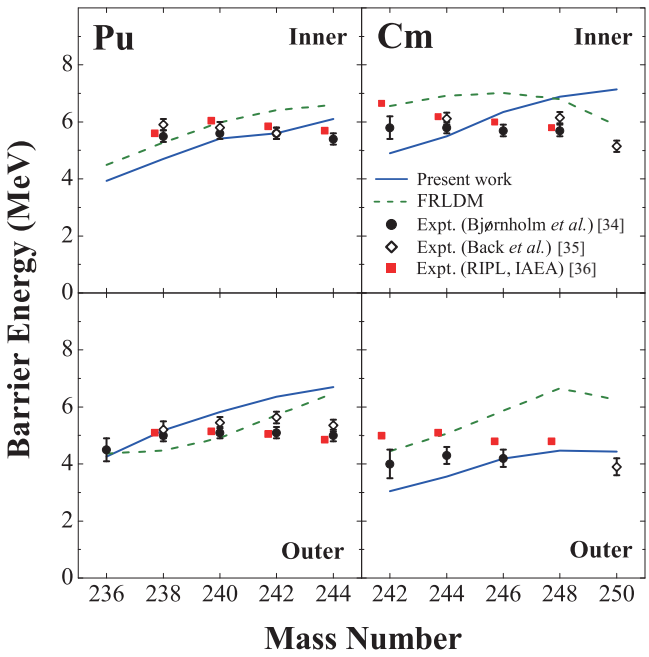

FIG. 1. (Color online) Calculated inner and outer fission-barrier heights for Pu and Cm isotopes, compared with experimental data [34–36] and the FRLDM calculations [37].

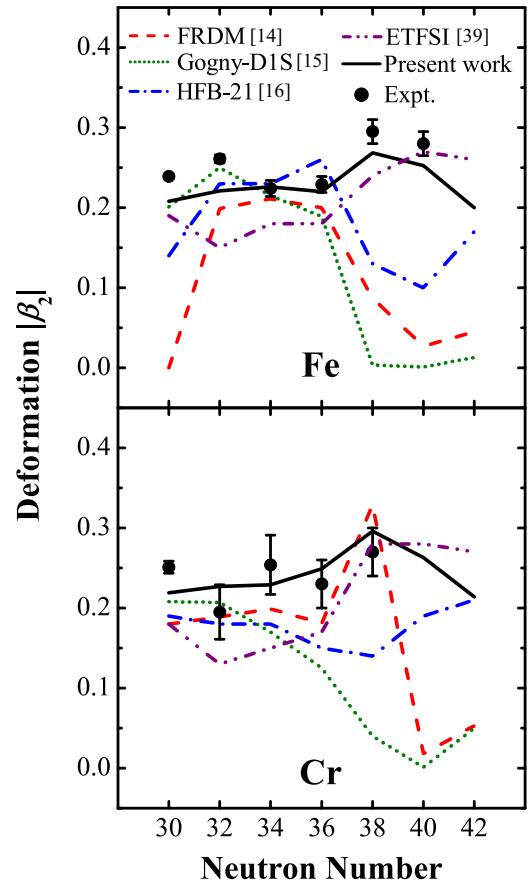

FIG. 2. (Color online) Ground-state β_2 deformations for neutron-rich Fe and Cr isotopes. The present results are shown as black solid lines, compared with the previous mean-field calculations [14–16,39] and experimental data [38].

have calculated two-humped fission barriers for Pu and Cm isotopes in which experimental information has been available, shown in Fig. 1. It is seen that obtained barrier heights are in reasonable agreements with the values extracted from experiments [34–36] and the calculations by the finite-range liquid-drop model (FRLDM) [37]. Since the projected PES calculations are restricted to (β_2,β_4) deformation, one may expect that the description of fission barriers would be further improved with inclusion of the axially asymmetric γ and reflection-asymmetric β_3 deformations.

III. CALCULATIONS AND DISCUSSIONS

As noted in the Introduction, experiments indicate enhanced collectivities in $^{64-68}$Fe and ^{62,64}Cr [11–13], while mean-field calculations which break the rotational symmetry gave reduced collectivities in neutron-rich Fe and Cr isotopes near $N = 40$ [14–16]. This region thus provides a good testing ground to study effects arising from the rotational-symmetry restoration. Figure 2 plots our calculated ground-state deformations for $^{56-68}$Fe and $^{54-66}$Cr, compared with experimental data [38]. Our results exhibit a remarkably increasing trend in deformations towards $N = 40$, reproducing well the experimental values. We see that the majority of mean-field calculations

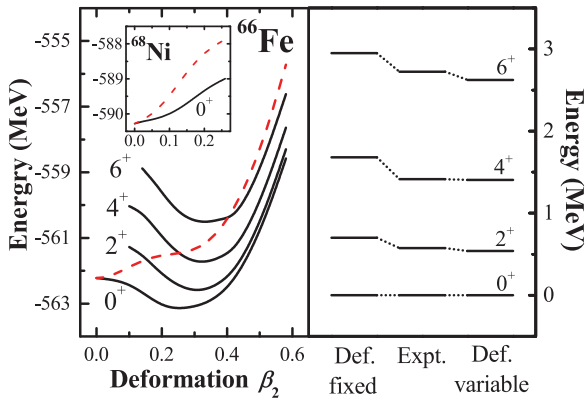

FIG. 3. (Color online) Left panel: Angular-momentum-conserved (projected) PES's at different spins for the ^{66}Fe ground-state band. At each β_2 value, the energy has been minimized with respect to the β_4 deformation. The dashed line indicates the calculation without the angular-momentum projection. Inset: The PES's of the ^{68}Ni ground state with and without the angular-momentum projection. Right panel: The level scheme of the ^{66}Fe ground-state band calculated with fixed and variable deformations, compared with data [7].

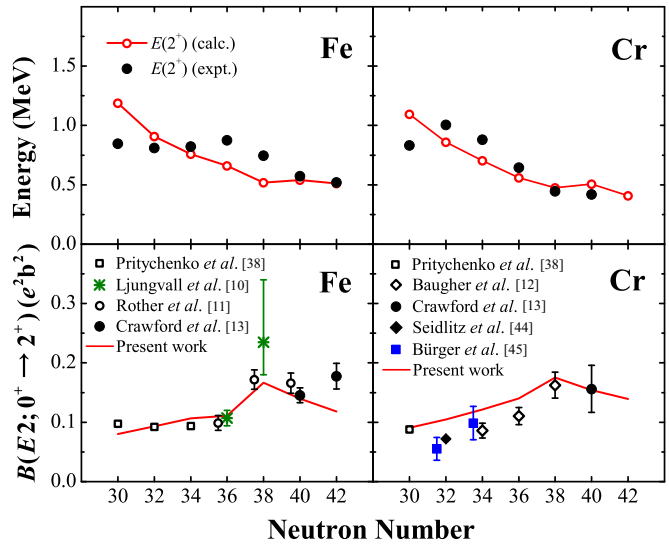

FIG. 4. (Color online) Calculated excitation energies of the 2_1^+ and 4_1^+ states (upper panels) and $B(E2; 0_1^+ \rightarrow 2_1^+)$ values (lower panels) for neutron-rich Fe and Cr isotopes, compared with experimental data taken from National Nuclear Data Center (NNDC) [43] and Refs. [10–13,38,44,45].

give decreased deformations when neutron number approaches 40. Only the extended Thomas-Fermi plus Strutinsky integral (ETFSI) method [39] and the present calculations show the increased deformations in both Fe and Cr isotopes when approaching $N = 40$. In the ETFSI model [40], a phenomenological rotational correction, $E_{\rm rot} = -\langle \hat{\mathbf{J}}^2 \rangle/(2\mathcal{J})$, has been added, where $\hat{\mathbf{J}}$ is the angular-momentum projector and $\mathcal{J}$ is the moment of inertia fitted to the experimental level spectra [40]. The $\langle \hat{\mathbf{J}}^2 \rangle$ is the expectation value calculated with the mean-field wave function [1,41]. The comparisons in Fig. 2 tell us that the effect from the rotational symmetry restoration is crucial to reproduce the experimental deformations of these nuclei.

A direct probe into deformation and associated collectivity is the γ-ray spectroscopy of a nucleus. A low-lying 2_1^+ state is considered as the fingerprint of a well-deformed shape. In the present work, we can obtain the energy of an excited state by minimizing the corresponding projected PES at the given spin. As an example, Fig. 3 displays the projected PES's at different spins for ^{66}Fe with the neutron number at the $N = 40$ subshell closure. The calculation without angular-momentum projection gives a spherical shape for the ground state, while the projection leads to a definite deformation for the semi-shell-closure nucleus, reproducing well the observation (see also the upper panel of Fig. 2). We see that the deformation (i.e., the location of the minimum) changes by increasing the angular momentum. The projected PES calculations give the excitation energies of 0.538 MeV for the 2_1^+ and 1.405 MeV for the 4_1^+ states in ^{66}Fe, agreeing well with the experimental values of 0.573 and 1.414 MeV [6].

In the right panel of Fig. 3, we plot the calculated level scheme of the ground-state band, showing the improvement of the calculations by the projected PES, compared with experimental data. The "standard" PSM itself [21] cannot give nuclear deformation by using the PES method if only the valence particles are taken into account in the calculation. Normally, the ground-state deformation obtained by nonprojected PES should be used for the deformation-fixed PSM calculation. In the ^{66}Fe case, however, the ground-state nonprojected PES gives a spherical deformation (see Fig. 3). A spherical shape cannot lead to any collective rotational band. In the deformation-fixed PSM calculations of the level scheme in Fig. 3, we take the deformation parameters given by the ground-state projected $I = 0$ PES (which are $\beta_2 = 0.253$ and $\beta_4 = 0.009$). One may question if the projected PES would always give a deformed shape. The inset of Fig. 3 shows the PES's of the ground state for another $N = 40$ nucleus ^{68}Ni, calculated with and without the angular-momentum projection. Both calculations give a spherical deformation. The spherical shape has been supported by the experimental observation [42].

Figure 4 gives the calculated excitation energies of the first 2^+ states for the Fe and Cr isotopes. In general, both calculated and experimental excitation energies decrease with increasing neutron number, implying increased collectivities when approaching $N = 40$. This phenomenon seems to be "abnormal." One would expect that the collectivity should be decreased when neutron number approaching a magic or semimagic number.

The reduced $E2$ transition probability $B(E2)$ provides another probe into the collectivity of a nucleus. The wave function Ψ^I defined in Eq. (1) allows us to calculate the $B(E2)$ value. The $B(E2)$ value from an initial state with spin $(I - 2)$ to a final state at spin I is given by

$$B(E2; I-2 \rightarrow I) = \frac{1}{2I-3} |\langle \Psi^I || e_\tau r^2 Y_2 || \Psi^{I-2} \rangle|^2, \quad (8)$$

where both Ψ^I and Ψ^{I-2} are obtained with the ground-state deformation determined by the projected PES. e_τ denotes

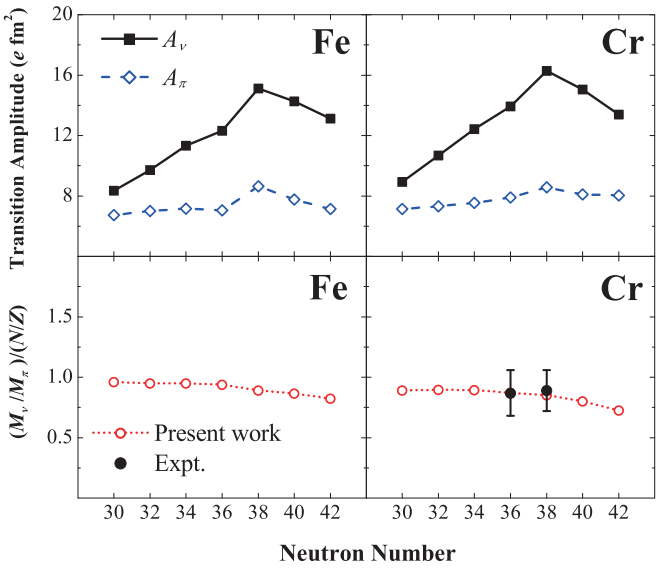

FIG. 5. (Color online) Calculated neutron and proton $E2$ transition amplitudes (upper panels) and neutron-to-proton ratios of transition matrix elements (lower panels) for the $2_1^+ \rightarrow 0_1^+$ transitions in neutron-rich Fe and Cr isotopes. Experimental data are taken from Ref. [12].

the effective charge with e_π and e_ν for proton and neutron, respectively. It was commented that the "standard" effective charges of $e_\pi = 1.5e$ and $e_\nu = 0.5e$ result in overestimated $B(E2)$ values in this mass region [11,12]. We therefore adopt the effective charges of $e_\pi = 1.31e$ and $e_\nu = 0.46e$ which can provide the better descriptions of the $B(E2)$ values [13]. As shown in the lower panels of Fig. 4, our calculations are in good agreement with experimental $B(E2)$ data.

It has been a subject of considerable interest what nucleus attains the maximum collectivity in this region near $N = 40$ [12,13]. Experimentally, Baugher *et al.* [12] pointed out that a saturation in collectivity has been reached in ^{62}Cr with $N = 38$. From the lower panels of Fig. 4, we see that both our calculations and experimental data indeed suggest the largest quadrupole collectivity in ^{62}Cr and ^{64}Fe with $N = 38$.

For a further analysis of the proton and neutron contributions to the $B(E2)$ values, we rewrite Eq. (8) by $B(E2; 0_1^+ \rightarrow 2_1^+) = 5(e_\pi A_\pi + e_\nu A_\nu)^2$ [12,13], where A_π and A_ν are the proton and neutron $E2$ transition amplitudes, respectively. We plot the calculated A_π and A_ν in the upper panels of Fig. 5. It is seen that the proton $E2$ transition amplitude A_π stays essentially constant in both Fe and Cr isotopes. By contrast, the neutron contribution increases significantly with increasing neutron number until $N = 38$. In general, these results are consistent with the large-scale shell-model calculations [13]. The present calculations give a peak at $N = 38$ for the neutron $E2$ transition amplitude, which should correspond to the peak of experimental $B(E2)$ data (see Fig. 4). However, the calculations seem to underestimate the $B(E2)$ value (or the $E2$ transition amplitude) of ^{68}Fe with $N = 42$, compared with data. This may indicate that the "standard" Nilsson parameters would not work well for nuclei far from the stability. The large-scale shell-model calculation gives a significant increase in the A_ν amplitude with neutron number increasing from $N = 36$ to $N = 40$ (38), and a smooth increase from $N = 40$ (38) to $N = 42$ in the Fe (Cr) chain [13]. The authors of Ref. [13] used an effective interaction which was tuned especially for this neutron-rich mass region [46], reproducing well the experimental $B(E2)$ value of the $N = 42$ neutron-rich Fe isotope [13].

We have also investigated the neutron-to-proton ratio of the transition matrix element M_ν/M_π (relative to N/Z). Since this quantity removes the dependence on nucleon numbers, it can be regarded as a "unified" criterion to evaluate collectivity in the whole nuclear chart [47,48]. M_ν/M_π is related to the neutron and proton deformation lengths (δ_ν and δ_π) via [47]

$$\frac{M_\nu}{M_\pi} = \frac{N\delta_\nu}{Z\delta_\pi}. \tag{9}$$

In the picture of the "pure" collective excitation, neutrons and protons have equal deformation lengths, resulting in $(M_\nu/M_\pi)/(N/Z) = 1$. In a nucleus with a closed neutron (proton) shell, valence protons (neutrons) dominate the low-lying excitation, which leads to $M_\nu/M_\pi < N/Z$ ($M_\nu/M_\pi > N/Z$) [47,48]. Experimentally, M_ν/M_π can be obtained by combining Coulomb excitation and proton scattering data [47]. In our calculations, the neutron and proton $E2$ transition matrix elements can be obtained by the generalized effective charge model [47,49], i.e., $M_\nu = A_\nu e_\pi + A_\pi e_\nu$ and $M_\pi = A_\pi e_\pi + A_\nu e_\nu$. From the lower panels of Fig. 5, we see that the calculated $(M_\nu/M_\pi)/(N/Z)$ values of the $2_1^+ \rightarrow 0_1^+$ transitions agree well with the existing data of 0.87(19) for ^{60}Cr and 0.89(17) for ^{62}Cr. All the calculated M_ν/M_π values are around $0.9(N/Z)$, indicating that the low-lying excitations follow the simple picture of the collective mode with nearly equal contributions from protons and neutrons in the investigated neutron-rich Fe and Cr nuclei.

IV. SUMMARY

By incorporating the angular-momentum projection into the macroscopic-microscopic model, we have developed the PES calculation which preserves a good angular momentum in the whole deformation lattice. Since the original liquid-drop model does not considered explicitly the problem of the angular-momentum conservation, we have calibrated the liquid-drop model parameters by refitting nuclear binding energies and tested by calculating fission barriers. The projected PES gives, in a self-consistent manner, the energy and deformation of a nuclear state at a given spin. Such calculations are particularly important for soft nuclei. By calculating projected PES's, we have investigated the quadrupole collectivities of neutron-rich Fe and Cr isotopes. It is found that the effect from the rotational-symmetry restoration is crucial to reproduce the experimental deformed shapes of the neutron-rich Fe and Cr isotopes, while usual mean-field calculations without considering the angular-momentum correction give spherical shapes. The calculated excitation energies and $E2$ transition probabilities of the 2_1^+ states are in reasonable agreement with experimental data. For the isotopes around $N = 40$, the large $B(E2)$ values obtained in both the present calculations and experiments indicate large deformations. The calculated

neutron-to-proton ratios of the $E2$ transition matrix elements are close to the limit of the collective motion, agreeing well with the existing data.

ACKNOWLEDGMENTS

We thank Y. Sun for providing the code of the PSM. Valuable comments from R. Wyss, P. Ring, W. Nazarewicz, Y. S. Chen, and Z. C. Gao are acknowledged. This work has been supported by the National Key Basic Research Program of China under Grant No. 2013CB83440; the National Natural Science Foundation of China under Grants No. 11235001, No. 11320101004, and No. 11375016; and the Open Project Program of State Key Laboratory of Theoretical Physics, Institute of Theoretical Physics, Chinese Academy of Sciences, China (No. Y4KF041CJ1).

[1] M. Bender, P.-H. Heenen, and P.-G. Reinhard, Rev. Mod. Phys. **75**, 121 (2003).
[2] M. Bender, G. F. Bertsch, and P.-H. Heenen, Phys. Rev. C **73**, 034322 (2006).
[3] R. Rodríguez-Guzmán, J. L. Egido, and L. M. Robledo, Phys. Lett. B **474**, 15 (2000).
[4] A. Valor, P.-H. Heenen, and P. Bonche, Nucl. Phys. A **671**, 145 (2000).
[5] R. R. Rodríguez-Guzmán, J. L. Egido, and L. M. Robledo, Phys. Rev. C **62**, 054319 (2000).
[6] M. Hannawald *et al.*, Phys. Rev. Lett. **82**, 1391 (1999).
[7] P. Adrich *et al.*, Phys. Rev. C **77**, 054306 (2008).
[8] A. Gade *et al.*, Phys. Rev. C **81**, 051304(R) (2010).
[9] N. Aoi *et al.*, Phys. Rev. Lett. **102**, 012502 (2009).
[10] J. Ljungvall *et al.*, Phys. Rev. C **81**, 061301(R) (2010).
[11] W. Rother *et al.*, Phys. Rev. Lett. **106**, 022502 (2011).
[12] T. Baugher *et al.*, Phys. Rev. C **86**, 011305(R) (2012).
[13] H. L. Crawford *et al.*, Phys. Rev. Lett. **110**, 242701 (2013).
[14] P. Möller, J. R. Nix, W. D. Myers, and W. J. Swiatecki, At. Data Nucl. Data Tables **59**, 185 (1995).
[15] S. Hilaire and M. Girod, Eur. Phys. J. A **33**, 237 (2007).
[16] S. Goriely, N. Chamel, and J. M. Pearson, Phys. Rev. C **82**, 035804 (2010).
[17] L. Gaudefroy, A. Obertelli, S. Péru, N. Pillet, S. Hilaire, J.-P. Delaroche, M. Girod, and J. Libert, Phys. Rev. C **80**, 064313 (2009).
[18] T. R. Rodríguez and J. L. Egido, Phys. Lett. B **705**, 255 (2011).
[19] T. R. Rodríguez and J. L. Egido, Phys. Rev. C **84**, 051307(R) (2011).
[20] Y. Sun, X. R. Zhou, G. L. Long, E. G. Zhao, and P. M. Walker, Phys. Lett. B **589**, 83 (2004).
[21] K. Hara and Y. Sun, Int. J. Mod. Phys. E **04**, 637 (1995).
[22] Y. Sun, J.-Y. Zhang, and M. Guidry, Phys. Rev. Lett. **78**, 2321 (1997).
[23] Y. Sun, Y. C. Yang, H. L. Liu, K. Kaneko, M. Hasegawa, and T. Mizusaki, Phys. Rev. C **80**, 054306 (2009).
[24] Y. C. Yang and Y. Sun, Sci. China Phys. Mech. Astron. **54**, s81 (2011).
[25] C. F. Jiao, Y. Shi, F. R. Xu, Y. Sun, and P. M. Walker, Sci. China Phys. Mech. Astron. **55**, 1613 (2012).
[26] Y. Tu, Y. S. Chen, Z. C. Gao, S. Y. Yu, and L. Liu, Sci. China Phys. Mech. Astron. **57**, 2054 (2014).
[27] G. X. Dong, X. B. Wang, H. L. Liu, and F. R. Xu, Phys. Rev. C **88**, 024328 (2013).
[28] P. Möller and J. R. Nix, Nucl. Phys. A **536**, 20 (1992).
[29] W. Nazarewicz, J. Dudek, R. Bengtsson, T. Bengtsson, and I. Ragnarsson, Nucl. Phys. A **435**, 397 (1985).
[30] R. Wyss, W. Satuła, W. Nazarewicz, and A. Johnson, Nucl. Phys. A **511**, 324 (1990).
[31] K. Pomorski and J. Dudek, Phys. Rev. C **67**, 044316 (2003).
[32] W. D. Myers and W. J. Swiatecki, Nucl. Phys. **81**, 1 (1966).
[33] M. Wang, G. Audi, A. H. Wapstra, F. G. Kondev, M. MacCormick, X. Xu, and B. Pfeiffer, Chin. Phys. C **36**, 1603 (2012).
[34] S. Bjørnholm and J. E. Lynn, Rev. Mod. Phys. **52**, 725 (1980).
[35] B. B. Back, O. Hansen, H. C. Britt, and J. D. Garrett, Phys. Rev. C **9**, 1924 (1974).
[36] T. Belgya *et al.*, *Handbook for Calculations of Nuclear Reaction Data, RIPL-2, IAEA-TECDOC-1506* (IAEA, Vienna, 2006).
[37] P. Möller, A. J. Sierk, T. Ichikawa, A. Iwamoto, R. Bengtsson, H. Uhrenholt, and S. Åberg, Phys. Rev. C **79**, 064304 (2009).
[38] B. Pritychenko, J. Choquette, M. Horoi, B. Karamy, and B. Singh, At. Data Nucl. Data Tables **98**, 798 (2012).
[39] Y. Aboussir, J. M. Pearson, A. K. Dutta, and F. Tondeur, At. Data Nucl. Data Tables **61**, 127 (1995).
[40] J. M. Pearson, Y. Aboussir, A. K. Dutta, R. C. Nayak, and M. Farine, Nucl. Phys. A **528**, 1 (1991).
[41] A. Baran and W. Höhenberger, Phys. Rev. C **52**, 2242 (1995).
[42] O. Sorlin *et al.*, Phys. Rev. Lett. **88**, 092501 (2002).
[43] NuDat 2.6, http://www.nndc.bnl.gov/nudat2/.
[44] M. Seidlitz *et al.*, Phys. Rev. C **84**, 034318 (2011).
[45] A. Bürger *et al.*, Phys. Lett. B **622**, 29 (2005).
[46] S. M. Lenzi, F. Nowacki, A. Poves, and K. Sieja, Phys. Rev. C **82**, 054301 (2010).
[47] L. A. Riley *et al.*, Phys. Rev. C **72**, 024311 (2005).
[48] A. M. Bernstein, V. R. Brown, and V. A. Madsen, Phys. Lett. B **103**, 255 (1981).
[49] B. A. Brown and B. H. Wildenthal, Phys. Rev. C **21**, 2107(R) (1980).